

A few filters are enough: Convolutional Neural Network for P300 Detection

Montserrat Alvarado-González^{a,1}, Gibran Fuentes-Pineda^{b,1}, Jorge Cervantes-Ojeda^a

^a*Department of Applied Mathematics and Systems, Universidad Autónoma Metropolitana, 05348, Mexico City, Mexico*

^b*Department of Computer Science, Instituto de Investigaciones en Matemáticas Aplicadas y en Sistemas, Universidad Nacional Autónoma de México, 04510, Mexico City, Mexico*

Abstract

In this paper, we aim to provide elements to contribute to the discussion about the usefulness of deep CNNs with several filters to solve both within-subject and cross-subject classification for single-trial P300 detection. To that end, we present SepConv1D, a simple Convolutional Neural Network architecture consisting of a depthwise separable 1D convolutional block followed by a Sigmoid classification block. Additionally, we present a one-layer Fully-Connected Neural Network with two neurons in the hidden layer to show the unnecessary of having complex architectures to solve the problem under analysis. We compare their performances against CNN-based state-of-the-art architectures. The experiments did not show a statistically significant difference between their AUC. Moreover, SepConv1D has the lowest number of parameters of all by far. This is important because simpler, cheaper, faster and, thus, more portable devices can be built.

Keywords: Convolutional Neural Network, P300, single-trial, within-subject, cross-subject

1. Introduction

A Brain-Computer Interface (BCI) is a system composed of software and hardware that builds a channel of communication between the subject and the computer, using

*Corresponding author

Email address: amontserrat@gmail.com (Montserrat Alvarado-González)

¹These authors contributed equally to this work.

only the subject's brain signals [1]. The general process followed for a BCI can be divided into: subject's stimulation, acquisition of brain activity, signal preprocessing, feature extraction, classification, and translation of the output's classification into instructions to control an application or a device. One of the brain signals of interest in the community for controlling BCIs captured with the electroencephalogram (EEG) is the Event-Related Potential (ERP). In particular, the late P300 component has a stable temporal relationship with respect to the stimulation event, an interesting characteristic to control BCIs. For instance, it is related to cognitive and attention processes, and it is independent of the type of stimulation presented to the subject. The P300 is associated with the oddball paradigm, which consists in presenting a series of frequent stimuli interrupted by infrequent stimuli [2]. Thus, every time the infrequent stimulus is detected by the subject, his brain unconsciously generates a positive peak, approximately 300 ms after the stimulus.

Given that a BCI based on ERP signals is highly subject-specific, it requires two phases to be used: *i*) an offline training phase to calibrate the system for each subject, and *ii*) an online phase to actually let the subject control the BCI. For instance, the subject has to repeat several times the oddball paradigm increase the ERP's signal-to-noise ratio [3]. Since the stimulation process can become unacceptably slow and tiring for the subject, much of the effort in the BCI development is to stimulate the subject as few times as possible, preferably only once (i.e., by a single-trial), while still achieving an adequate detection of the P300 component. On the other hand, a great effort has also been made to eliminate the calibration stage for each subject by using instead the information acquired previously for other subjects. The P300 detection based on the information retrieved during the calibration stage by a single subject is known as within-subject classification, whereas the detection based on the information retrieved by other subjects is known as cross-subject classification.

In order to detect the P300 under these conditions, a large amount of feature extraction, feature selection, and classification methods have been developed or applied by the BCI community. Some of them rely on features specified manually that requires significant human expertise. Lotte et al. [4] explained that once extracted, the features are selected to: *i*) reduce redundancy, *ii*) choose the ones related to the mental states

targeted by the BCI, *iii*) generate fewer parameters to be optimized by the classifier, and *iv*) produce faster predictions for a new sample. The feature selection approaches that have been used are the embedded methods (e.g., Stepwise Linear Discriminant Analysis [5]) and the wrapper methods (e.g., Genetic Algorithms [6]). On the other hand, the approaches more commonly used for P300 classification are the Linear Discriminant Analysis [7], Support Vector Machines [8], Feed Forward Neural Networks [9, 10], and adaptive classifiers [11, 12].

However, new methods merge feature extraction, feature selection, and classification methods by using matrix classifiers [13] as well as Deep Learning with Convolutional Neural Networks (CNN). In particular, the latter has gained more interest since it has demonstrated to be very effective in fields such as Computer Vision [14] and Speech Recognition [15], not only to avoid hand-designed features but also to increase the classification rates. The main characteristics of these methods are their depth, the use of a large number of filters, and their need to train with large amounts of data. These characteristics may be a disadvantage for P300 detection, mostly due to the limited training data available [16, 4].

At the moment, there have been some CNN approaches that seem to be effective for P300 detection in BCI [17, 18, 19, 20, 21, 22]. However, the increase in classification rates has not been as impressive as in other areas and does not justify the depth of the architectures and the number of filters used. Nevertheless, one of their advantages is their potential to visualize features (e.g., the EEGNet [19]), which can be used to analyze the signals in more detail.

In this paper, we aim to provide elements to contribute to the discussion about the usefulness of deep CNNs with several filters to solve the problems already discussed. To that end, we propose a CNN algorithm that requires significantly fewer parameters than any of the state-of-the-art architectures with at least the same performance, the SepConv1D. Additionally, we describe a simple Fully-Connected Neural Network to show that it is not necessary to have complex architectures to solve the problem under analysis. Furthermore, we compare their performances against the state-of-the-art CNN methods for both within-subject and cross-subject classification for single-trial P300 detection.

The remainder of this paper is organized as follows. In Section 2, we describe the general components of a CNN and review the state-of-the-art methods used for P300 detection. In Section 3, we present the simple Fully-Connected Neural Network and the SepConv1D. In Section 4, we describe the experimentation protocol and data analysis. Section 5, shows the results of the classification performance and the discussion about them. Finally, in Section 6, we provide some concluding remarks.

2. Convolutional Neural Networks for the P300 detection

2.1. Components of Convolutional Neural Networks

A Convolutional Neural Network (CNN) is one of the most popular Deep Neural Network architectures. Goodfellow et al. [23] mentioned that one of the main differences between traditional and convolutional neural networks is that the former use a multiplication matrix while the latter use a convolution operation in at least one of its layers. This section gives a concise presentation of the main CNN's layers to extract and downsample features.

EEG signals

The EEG signals are recorded by C channels and discretized by T number of samples. The filtered signals are represented by a matrix \mathbf{X} of size $C \times T$, where each vector $\mathbf{x}_c = [x_1, \dots, x_T]$ represents the EEG signals recorded by a single channel $c = 1, \dots, C$.

We apply channel-wise feature scaling to standardize the values of the filtered signal of each channel separately as follows:

$$\mathbf{x}'_c = \frac{(\mathbf{x}_c - \mu(\mathbf{x}_c))}{\sigma(\mathbf{x}_c)}, \quad (1)$$

where μ and σ are the mean and standard deviation of the channel c , defined by Eq.(2) and Eq.(3) respectively:

$$\mu(\mathbf{x}) = \frac{1}{|\mathbf{x}|} \sum_{t=1}^{|\mathbf{x}|} x_t, \quad (2)$$

$$\sigma(\mathbf{x}) = \frac{1}{|\mathbf{x}|} \sum_{t=1}^{|\mathbf{x}|} (x_t - \mu(\mathbf{x}))^2. \quad (3)$$

Convolutional layers

Most of the architectures under analysis have at least two convolutional layers. Typically, one of them serves as a spatial filtering layer, which represents a spatial distribution across the scalp [18, 21]. In most cases, the second layer finds temporal patterns in the signal representing the change in amplitude of the spatial maps learned in the first layer [18]; however, in some cases [20, 19], the second layer builds feature maps containing different band-pass frequencies.

In general, a convolution layer is represented as follows. Let $\mathbf{Y}^{(l)}$ denote the matrix of outputs from layer l , where $\mathbf{Y}^{(0)} = \mathbf{X}'$, the input matrix of the scaled and, optionally, filtered EEG signals. In order to extract the features of interest, the convolutional layer convolves each input matrix $\mathbf{Y}^{(l)}$ with a bank of $1 \dots f \dots F$ filters. The convolutional layer applies a convolution operation that can be expressed as:

$$z_{f,t}^{(l+1)} = \sum_{j=1}^J \sum_{i=1}^I y_{f,t}^{(l)} \cdot w_{f,j,t-i}^{(l+1)} + b_f^{(l+1)}, \quad (4)$$

$$y_{f,t}^{(l+1)} = h(z_{f,t}^{(l+1)}), \quad (5)$$

where $\mathbf{y}_f^{(l+1)} = [y_{f,1}^{(l+1)}, \dots, y_{f,T}^{(l+1)}]$ is the row vector representing the output feature map associated with each filter f , at a sample t , $b_f^{(l+1)}$ is the bias, and h is the activation function (see below).

Batch Normalization

Ioffe and Szegedy [24] proposed the Batch Normalization (BN) algorithm to accelerate the training's convergence speed and to reduce the difficulty of parameter initialization by adjusting and scaling the activations.

The Batch Normalization process is described as follows. For a layer with J -dimensional input $\mathbf{Z}^{(l)}$, each dimension is normalized as follows:

$$z'_{j,i} = \frac{z_{j,i} - \mu(\mathbf{z}_j)}{\sqrt{\sigma(\mathbf{z}_j)^2 + \epsilon}}, \quad (6)$$

where ϵ is a small positive number added to the mini-batch variance $\sigma(\mathbf{z}_j)^2$ for numerical stability [24]. Finally, the normalized vector is scaled and shifted as follows:

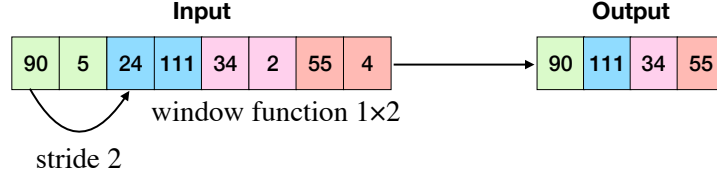


Figure 1: Max-Pooling example. A window function of 1×2 moves through the input vector every two elements. The input's elements overlapping this function are compared between them to maintain the maximum element.

$$\hat{z}_{j,i} = \gamma z'_{j,i} + \beta, \quad (7)$$

where γ and β will be optimized together with the weights and biases of the network. Batch Normalization should be performed before applying the activation function to avoid the distribution shift, which leads to saturation and decelerates learning.

Pooling

Most architectures use a pooling function to reduce the dimensionality of the vector or to reduce the sampling rate of the signal. It can be either Average or Max-pooling.

The Pooling process downsamples the input $\mathbf{y}^{(l)}$, reducing the dimensionality of the feature vector. The Max-Pooling function applies a window function $u(x, y)$ to an input patch of the vector's elements, and computes the maximum value. Then, the window is moved P strides and the operation is repeated. Figure 1 shows an example of Max-Pooling with a window function of 1×2 . The Max-Pooling is defined by Scherer et al. [25] as:

$$\mathbf{y}^{(l+1)} = \max(\mathbf{y}^{(l)(1 \times P)} u(1, P)). \quad (8)$$

The Average-Pooling operation is similar to the Max-Pooling, however, instead of getting the highest value, it computes the average value of the overlapped elements.

Activation Functions

In what follows, we describe the activation functions used by the analyzed models.

- The Linear activation function is a polynomial of one degree, which is limited in its learning power of complex functional mappings. It is defined as

$$h(z_i^{(l)}) = \gamma z_i^{(l)}, \quad (9)$$

where γ is the slope.

- The *Log* activation function is a logarithmic function bounded in a range of $[1e-7, 10000]$.

$$h(z_i^{(l)}) = \log(z_i^{(l)}). \quad (10)$$

- The Square activation function does not have a stable range since they explode in magnitude quickly. Since its output is a big value, this function tends to result in bad generalization. Additionally, it takes longer to converge than other activation functions. It is defined as

$$h(z_i^{(l)}) = z_i^{(l)2}. \quad (11)$$

- The Sigmoid activation function is a sigmoidal function in the range $[0, 1]$. It usually has a slow convergence given by the fading of the gradient in deep networks. When the network is not very deep, it converges quickly. It is defined as

$$h(z_i^{(l)}) = \frac{1}{1 + e^{-z_i^{(l)}}}. \quad (12)$$

- The Hyperbolic Tangent activation function (*tanh*) is a sigmoidal function in the range $[-1, 1]$ which is "sometimes preferred, partly because it has a steady-state at 0" [26]. It is defined as

$$h(z_i^{(l)}) = \tanh(z_i^{(l)}) = \frac{e^{2z_i^{(l)}} - 1}{e^{2z_i^{(l)}} + 1}. \quad (13)$$

- The Scaled Hyperbolic Tangent activation function (*stanh*) [27] is a sigmoidal function in the range $[-1, 1]$ whose advantage is that the negative inputs will be mapped strongly negative and the zero inputs will be mapped near zero. It is defined as

$$h(z_i^{(l)}) = 1.7159 \tanh\left(\frac{2}{3} z_i^{(l)}\right). \quad (14)$$

- The Softmax activation function [23] turns scores into probabilities that sum to one. It is defined as

$$h(z_i^{(l)}) = \frac{e^{z_i^{(l)}}}{\sum_j e^{z_j^{(l)}}. \quad (15)$$

- The Rectified Linear Unity (ReLU) alleviates the vanishing and exploding gradient problems that are usually associated with saturated activation functions such as Sigmoid or *tanh*. The activation function rectifies the net inputs \mathbf{z} , by setting the negative values to zero and by keeping the positive values [28], enabling a faster convergence during the training stage:

$$h(z_i^{(l)}) = \max(0, z_i^{(l)}). \quad (16)$$

- Similarly to ReLU, the Exponential Linear Units (ELU) [29] alleviate the vanishing gradient problem via the identity for positive values. Clevert et al. claimed that ELU leads to faster learning, and to significantly better generalization performance than ReLU on networks with more than five layers. They have negative values allowing them to push mean unit activations closer to zero:

$$h(z_i^{(l)}) = \begin{cases} z_i^{(l)} & \text{if } z_i^{(l)} > 0 \\ \phi(e^{z_i^{(l)}} - 1) & \text{if } z_i^{(l)} \leq 0 \end{cases}. \quad (17)$$

The ELU hyperparameter ϕ controls the value to which an ELU saturates for negative net inputs.

Dropout

Dropout is a regularization technique to prevent overfitting the neural network during the training stage (see Figure 2); it is defined by Srivastava et al. [30] as follows:

$$r_j^{(l)} \sim \text{Bernoulli}(p), \quad (18)$$

$$\mathbf{y}'^{(l)} = \mathbf{r}^{(l)} * \mathbf{y}^{(l)}, \quad (19)$$

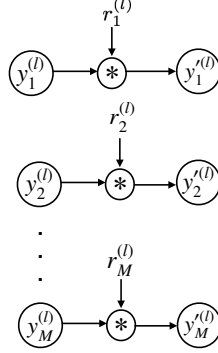


Figure 2: Example of the Dropout process: $r_j^{(l)}$ is a random variable which has probability p of being 1. Only when $r_j^{(l)} = 1$, $y_j'^{(l)}$ will be taken into account.

where $r_j^{(l)}$ is an independent Bernoulli random variable which has a probability p of being 1, and $*$ denotes the Hadamard product between the vector $\mathbf{r}^{(l)}$ and the outputs of the layer $\mathbf{y}^{(l)}$, to get the sampled outputs of the layer $\mathbf{y}'^{(l)}$.

Fully Connected Block (Dense)

The features-maps of the last convolutional block's output is vectorized. The resulting vector is fed into a fully connected layer. Each layer is defined as:

$$z_i^{(l+1)} = \mathbf{w}_i^{(l+1)} \mathbf{y}^{(l)} + \mathbf{b}_i^{(l+1)}, \quad (20)$$

$$y_i^{(l+1)} = h(z_i^{(l+1)}), \quad (21)$$

where $\mathbf{W}^{(l)}$ and $\mathbf{B}^{(l)}$ are the weights and biases at layer l ; and h is an activation function (see Section 2.1).

Optimizer

In order to update the network weights and biases, the architectures applied the Adaptive Moment Estimation (Adam), a stochastic-based gradient optimization with adaptive learning rates [31]. Given all the network's parameters θ , which include all the weights and biases, the update rule at the training step k is given by:

$$\theta^{(k)} = \theta^{(k-1)} - \eta \cdot \hat{\mathbf{m}}^{(k)} / (\sqrt{\hat{\mathbf{v}}^{(k)}} + \alpha), \quad (22)$$

where \oslash denotes the element-wise division, α is a very small number to avoid any division between zero, η is the learning rate, and $\hat{\mathbf{m}}^{(k)}$ and $\hat{\mathbf{v}}^{(k)}$ are bias-corrected estimates of the first and second moment of the gradients respectively. These estimates are calculated by using exponentially weighted moving averages as follows:

$$\mathbf{m}^{(k)} = \beta_1 \mathbf{m}^{(k-1)} + (1 - \beta_1) \mathbf{g}^{(k)}, \quad (23)$$

$$\mathbf{v}^{(k)} = \beta_2 \mathbf{v}^{(k-1)} + (1 - \beta_2) (\mathbf{g}^{(k)} * \mathbf{g}^{(k)}), \quad (24)$$

where β_1 and β_2 are exponential decay rates of the first and second moment respectively and $\mathbf{g}^{(k)}$ is the gradient of the loss function with respect to the parameters. Bias correction of the estimates is obtained by

$$\hat{\mathbf{m}}^{(k)} = \mathbf{m}^{(k)} / (1 - \beta_1), \quad (25)$$

$$\hat{\mathbf{v}}^{(k)} = \mathbf{v}^{(k)} / (1 - \beta_2). \quad (26)$$

Categorical cross entropy is defined for a set of M predictions \mathbf{y} with corresponding true outputs \mathbf{d} as

$$\mathcal{L}(\mathbf{y}, \mathbf{d}) = - \sum_{i=1}^M \{d_i \log(y_i) + (1 - d_i) \log(1 - y_i)\}. \quad (27)$$

The parameters are updated for each mini-batch of m examples in the training set. This process is repeated until having traversed the whole training set a predefined number of times (i.e., the number of epochs) or reaching a convergence condition. The hyperparameters are set as follows: $\alpha = 0.001$, $\beta_1 = 0.9$, $\beta_2 = 0.999$ and $\epsilon = 10^{-8}$, which are the values recommended by the authors of [31].

To initialize the weights of all the network, it is a common practice to use the Xavier Glorot uniform scheme [32]. This scheme draws samples from a uniform distribution in the interval $\left[-\frac{\sqrt{6}}{\sqrt{I+O}}, \frac{\sqrt{6}}{\sqrt{I+O}}\right]$, where I and O are the input and output units in the weight tensor, respectively. Additionally, biases and first and second moment estimates are initialized with zeros.

2.2. State-of-the-art CNN architectures to detect P300

CNN-1. Cecotti et al. [17] proposed a five-layer architecture, the first CNN for P300 detection. The first layer is a 1D-convolution in the space domain representing spatial filters. The second layer is a 1D-convolution over time which subsamples and filters the signals; it is composed of five maps with six neurons each. The third layer is composed of one map of 100 neurons; together with layers two and four, it builds a dense classification layer. The learning algorithm for tuning the weights of the network uses backpropagation. Table A.6 shows further details about the architecture. Additionally, the authors presented the CNN-3, a CNN-1 architecture with one filter in its first 1D-convolutional layer, in contrast to the 10 filters of the CNN-1. See Table A.7 to compare the differences in the number of parameters and the outputs of the layers. On the other hand, in order to upgrade both architectures, we implemented two modifications: *i)* we changed from two Sigmoids (one in each output neuron) to one Softmax, and *ii)* we changed the loss function from Mean Square Error to Binary Cross Entropy. We named the modified CNN-1 as UCNN-1 and the CNN-3 as UCNN-3.

CNN-R. Manor and Geva [18] proposed a more complex architecture, containing two convolutional-pooling blocks, a convolutional layer, two fully connected layers, followed by a Softmax-dense classification layer. The first convolutional block performs a spatial convolution. The weights of this layer are regularized with a spatio-temporal penalty that makes the filters smoother and more stable in time. The second convolutional block finds temporal patterns in the signal that represent the change in amplitude of the spatial maps learned in the first block. The network is trained by minimizing the Binary Cross-entropy loss function. The gradient is computed with the backpropagation algorithm. Table A.8 depicts the detailed CNN-R’s architecture.

Deep ConvNet. Schirrneister et al. [20] proposed a general-purpose architecture consisting of four convolutional blocks followed by a Softmax-dense classification layer. The first convolutional block is split into two layers: in the first layer, each filter performs a convolution over time, and in the second layer, each filter performs a spatial filtering with weights for all possible pairs of electrodes with filters of the preceding temporal convolution. It is followed by three standard convolutional-max-pooling

blocks. The architecture uses ELU as the activation function. Table A.9 shows further details about the architecture.

Shallow ConvNet. Additionally to the Deep ConvNet, Schirrmester et al. [20], presented an architecture originally designed to decode band-power features. The first two layers perform a temporal convolution and a spatial filter. They are followed by a squaring nonlinearity, a mean pooling layer, and a logarithmic activation function. The model ends with a Softmax-dense classification layer. See Table A.10 for more details about the architecture.

BN³. Liu et al. [21] proposed a six-layer architecture that combines Batch Normalization and Dropout techniques that is less susceptible to overfitting and faster in training than CNN-1. First, it is applied a 1D convolutional layer for spatial feature extraction. Followed by a 1D convolutional and subsampling layer for temporal feature extraction. Then, the architecture uses two fully-connected layers for better generalization and accumulation of features. The model uses the binary cross-entropy as the loss function and the gradient descent as the optimizer. Table A.11 depicts details about the architecture.

EEGNet. Lawhern et al. [19] proposed a compact CNN architecture consisting of two convolutional blocks followed by a Softmax classification block. The first convolutional block decomposes the EEG signal at different band-pass frequencies and reduces the number of trainable parameters by a depthwise convolution. The architecture applies batch normalization along with the feature map dimension before applying the ELU nonlinearity. The second convolutional block uses a separable convolution, which is a depthwise convolution followed by some pointwise convolutions, to reduce the number of parameters and to decoupling the relationship of feature maps. See Table A.12 for more details about the architecture.

OCLNN. Shan et al. [22], noted that the aforementioned CNNs needed deep and wide network architectures given that they were unable to learn temporal features properly. They claimed that CNNs' first layer outputs abstract instead of raw temporal signals,

losing useful temporal information to detect P300. They proposed a one-convolution-layer architecture, to reduce the network complexity, and obtained a better performance.

It is the simplest CNN architecture that had been presented so far. It consists of a 1D convolutional block followed by a Softmax classification block. The convolutional block divides the temporal signals from the input channels into 15 parts and performs a convolutional operation on each one for temporal and spatial feature extraction. Then, a Dropout is applied to reduce overfitting. See Table A.13 for more details about the architecture.

3. Methods

As previously explained, we would like to provide an alternative to highly complex architectures to detect P300. To that end, we now describe the low-cost CNN-based algorithm we propose, the SepConv1D. Additionally, we describe the 1-layer Fully-Connected Neural Network.

3.1. SepConv1D

Based on the OCLNN, the proposed architecture is a simple CNN architecture consisting of a depthwise separable 1D convolutional block followed by a Sigmoid classification block (see Figure 3). The main difference with the OCLNN is that SepConv1D uses a depthwise convolution to reduce the number of trainable parameters, while OCLNN uses a 1D convolutional block. This kind of convolution has been used successfully before by the EEGNet architecture. We used the hyperbolic tangent sigmoid activation function in the convolutional block. On the other hand, OCLNN connects two neurons to a Softmax function in the dense layer and applies a Dropout; in contrast, SepConv1D connects a single neuron to a Sigmoid function and does not apply a Dropout. In order to decide the number of filters to be used in the convolutional layer, we performed some experiments that will be explained in Section 5.

3.2. FCNN

The 1-layer Fully-Connected Neural Network (FCNN) we propose is similar to the one presented by [9] (see Figure 4). We used the hyperbolic tangent sigmoid

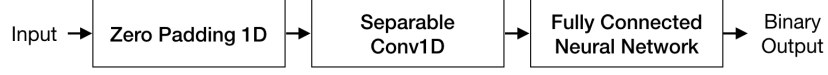


Figure 3: SepConv1D, a CNN architecture consisting of a depthwise separable 1D convolutional block followed by a Sigmoid classification block. Tables 2 and 4 show further detail about the architecture.

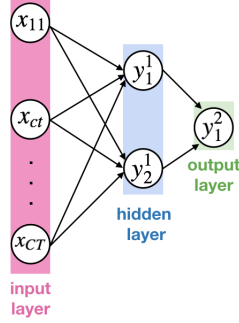


Figure 4: Three-layer Fully-Connected Neural Network composed of an input, a two-neuron hidden layer, and an output layer.

activation function in the hidden layer and a Sigmoid function in the output layer. After several experiments, we identified that the FCNN needs only two neurons in the hidden layer to obtain the best results. Thus, the layer's output is as follows: $y_1^2 = h\left(\sum_{j=1}^2 w_{j1}^{(1)} y_j^1 + b^{(1)}\right)$, where $w_{j1}^{(1)}$ is the connection weight from neuron j in layer (1) to output 1, and $b^{(1)}$ is the bias. The hidden layer's output is as follows: $y_j^1 = h\left(\sum_{i=0}^{C-T} w_{ij}^{(0)} x_i + b^{(0)}\right)$, where $w_{ij}^{(0)}$ is the connection weight from input i in layer 0 to intermediate neuron j , $x_0 = 1$ for all data samples, and x_i is an element of the matrix $\mathbf{X}' = [\mathbf{x}'_1^T, \mathbf{x}'_2^T, \dots, \mathbf{x}'_C^T]$. We modeled the presence of the P300 signal with $y = 1$ and the absence of the signal with $y = 0$. See Table 1 for more details about the architecture.

Layer	No. filters	No. params	Output	Activation function
Input Reshape Dense Flatten	2	2,474	6×206 1236×1 (2) (2)	\tanh
Dense	1	3	(1)	Sigmoid

Table 1: FCNN architecture.

4. Experimental Design

As we explained earlier, we aim to compare the performance of both within-subject and cross-subject classification of P300 single-trial of the aforementioned state-of-the-art CNN methods against a simple FCNN. In what follows, we explain in detail the experimental design.

4.1. Dataset

For our experiments, we used the EEG-signal dataset reported in [33]. Such dataset is composed of the EEG signals of 22 healthy students from 21 to 25 years old without known neurological damage.

4.2. Data Acquisition and Processing

The EEG-signal dataset was acquired by the use of 10 channels (Fz, C4, Cz, C3, P4, Pz, P3, PO8, Oz, and PO7) following the international 10-20 system, with the right earlobe and the right mastoid serving as reference and ground locations. However, we only used six of them (Fz, Cz, Pz, PO8, Oz, and PO7), since it has been previously reported [34] to be the most relevant to detect the P300 component. The signal was digitized at a rate of 256 Hz and processed online with a notch filter (Chebyshev of order 4), with cutoff frequencies between 58 and 62 Hz, and a bandpass filter (Chebyshev of order 8), with cutoff frequencies between 0.1 and 60 Hz.

4.3. Task Description and ERP Signal Extraction

The subjects were visually stimulated with the Donchin speller matrix described in [2]. The speller is a 6×6 matrix composed of alphanumeric symbols that allow the subjects to write a word. In order to generate the oddball paradigm, the rows and columns of the matrix flashed randomly 15 times every 125 ms (i.e., trials); each flash lasted 62.5 ms. The subjects were asked to silently count the number of times the target character was intensified. We extracted segments of 800 ms of EEG data after every stimulus. Each segment was filtered offline using a 4th-order Butterworth bandpass filter with bandwidth range from 0.1 to 12 Hz to extract the ERP signals embedded in the EEG. The DC component was removed by subtracting the mean of each electrode from the filtered signal. Finally, the linear trend was removed from each trial.

4.4. Evaluation

For the experiments, we set the number of training iterations over the neural networks to 50, because most of the models converged around that iteration. We ran 200 training iterations (epochs) and perform early stopping for all the architectures under analysis. Additionally, we fit the model using Adam optimizer, using default parameters as described in [31]. Trying to reproduce the architectures as closely as possible to their original descriptions, we minimized the Categorical Cross-Entropy loss function, except for the BN³, FCNN, and SepConv1D architectures that use Binary Cross Entropy.

For the within-subject classification experiments, we performed a five-fold cross-validation repeated 10 times for every subject’s data. Each repetition produced a split consisting of a training set with 80% of the data of a given subject and a validation set with the remaining 20%. On the other hand, for the cross-subject classification experiments, we used data from other subjects to train a subject model. To that end, we performed a leave-two-out cross-validation. Thus, we randomly chose one subject to test, another one to validate, and all remaining subjects for the training set. This process was repeated for each subject, producing 22 folds.

During training, we applied a sample weight when computing the loss function in order to cope with the class imbalance. For each model, we computed the *Area Under the Curve* (AUC) of the Receiver Operating Characteristic using the balanced validation set.

Finally, we perform statistical testing using a one-way analysis of variance (ANOVA) to determine the differences between classifiers under analysis.

4.5. Implementation details

The experiments were performed on a single PC with Linux Ubuntu 16.04, 64 GB in RAM and an NVIDIA GeForce GTX 1080 GPU with 2560 CUDA cores and 10 GB of RAM. P300-CNNT is implemented with the Keras API [35] of Tensorflow 1.8.0 [36]. The code of all the architectures under analysis is available at the following URL: <https://github.com/gibranfp/P300-CNNT>.

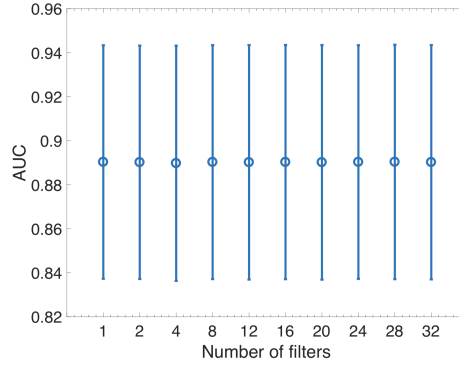


Figure 5: Mean AUC comparison of a different number of filters used by the SepConv1D for a within-subject classification.

Layer	No. filters	Size	No. params	Output	Activation function	Options
Input		206×6				
ZeroPadding1D				(214, 6)		padding = 4
SeparableConv1D	1	kernel = 16, stride = 8	103	(25, 1)		
Activation				(25, 1)	<i>tanh</i>	
Flatten				(25)		
Dense	1		26	(1)	Sigmoid	

Table 2: SepConv1D architecture for within-subject classification.

5. Results and Discussion

5.1. Within-subject classification

Selection of the number of filters for the SepConv1D

In order to obtain a balance between a low computational cost and the best performance, we carried out a series of experiments varying the number of filters used by the SepConv1D’s convolutional layer. To that end, we vary the filters from 1 to 32 in increments of four. Figure 5 shows that the mean value of AUC is very similar in all cases. For this reason, we decided to use only one filter for subsequent experiments to test the within-subject classification. See Table 2 for more details about the resulting architecture. The amount of trainable parameters for this model is 129. In what follows, we will call this architecture SepConv1D-1F. Figure 6 shows the resulting AUCs for the 22-subject dataset by using the SepConv1D-1F for within-subject classification.

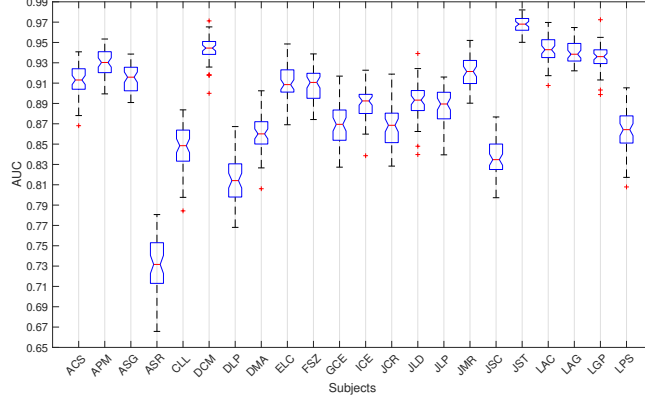


Figure 6: Resulting AUCs for the 22-subjects by using the SepConv1D-1F for within-subject classification.

Comparison with state-of-the-art CNN-based architectures

Given the previous results, we compare the performance of both FCNN and SepConv1D-1F with the CNN-based reference methods. Table 3 presents the mean AUC values of the within-subject five-fold cross-validation results across all methods, which can be seen in Figure 7.

The ANOVA analysis showed that the means AUCs of CNN3 and UCNN3 are significantly different from the rest of the methods.

The means AUCs of CNN-1 are very similar to those of CNN-R. However, in [18], the authors claimed that CNN-R performed significantly better than CNN-1.

On the other hand, the mean AUC values of Shallow ConvNet are significantly different from the means of Deep ConvNet but not from other methods. In contrast, in [19], the authors reported that they did not perform significantly different amongst themselves.

More importantly, the means of FCNN and SepConv1D-1F are not significantly different from other methods. Moreover, they are very similar to them.

5.2. Cross-subject classification

Selection of the number of filters for the SepConv1D

Similarly to the previous section, we carried out a series of experiments varying the number of filters used by the SepConv1D’s convolutional layer to find a compro-

Architecture	Within-subject classification AUC	Cross-subject classification AUC
CNN1	0.8961±0.05	0.8116±0.53
UCNN1	0.8922±0.05	0.8392±0.59
CNN3	0.7191±0.07	0.7734±0.13
UCNN3	0.7709±0.07	0.8239±0.62
CNN-R	0.8756±0.06	0.8319±0.58
Deep ConvNet	0.8973±0.05	0.8351±0.59
Shallow ConvNet	0.8344±0.08	0.8248±0.65
BN ³	0.8830±0.05	0.8375±0.57
EEGNet	0.8875±0.05	0.8398±0.60
OCLNN	0.8909±0.05	0.8317±0.59
FCNN	0.8913±0.05	0.8283±0.57
SepConv1D	0.8903±0.05	0.8361±0.59

Table 3: Mean and standard deviation AUCs of the architectures under analysis for both Within-subject and Cross-subject classifications.

Layer	No. filters	Size	No. params	Output	Activation function	Options
Input ZeroPadding1D SeparableConv1D	8	206 × 6 kernel = 16, stride = 8	152	(214, 6) (25, 8)		padding = 4
Activation Flatten Dense	1		201	(25, 8) (200) (1)	<i>tanh</i> Sigmoid	

Table 4: SepConv1D architecture for cross-subject classification.

mise between performance and low cost. Figure 8 shows that from eight filters both the mean AUC values and their standard deviations tend to stabilize. For this reason, we decided to use eight filters for subsequent experiments to test cross-subject classification. See Table 4 for more details about the resulting architecture. The amount of trainable parameters for this model is 353. In what follows, we will call this architecture SepConv1D-8F.

To understand the reason that more filters are required for cross-subject than for within-subject classification, we analyzed in detail the subject’s AUC means (see Figure 9). We do not observe significant differences between them, except for subjects DLP and JSC. Given that they require seven more filters, below we present a deeper analysis of the features learned in each filter.

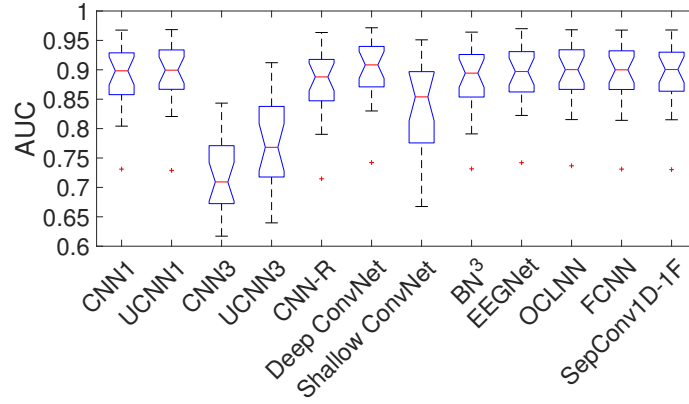


Figure 7: Mean AUC comparison between the models under analysis for within-subject classification. See detail in Table A.14.

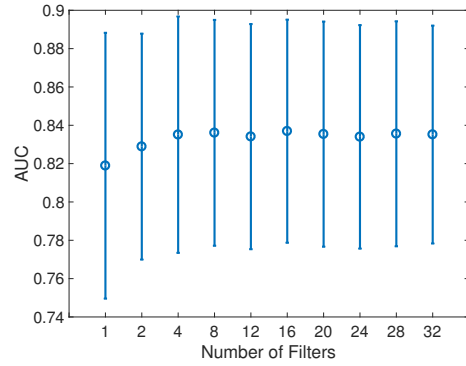


Figure 8: Mean AUC comparison for a different number of filters for the SepConv1D for a cross-subject classification.

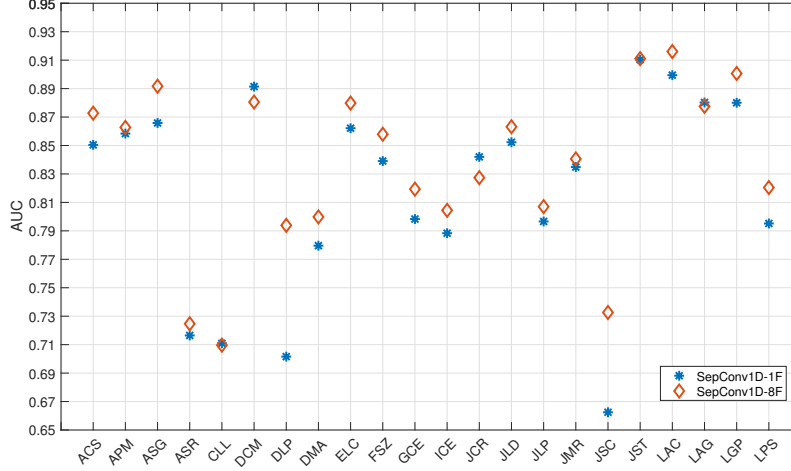


Figure 9: Resulting AUCs for the 22-subjects by using the SepConv1D-1F and SepConv1D-8F architectures for cross-subject classification.

Comparison with state-of-the-art CNN-based architectures

Given the previous results, we compare the performance of both FCNN and SepConv1D-8F with the CNN-based reference methods. Table 3 present the mean AUC values of the cross-subject classification across all methods, which can be seen in Figure 10. The ANOVA analysis showed that there is not a statistically significant difference between none of the methods ($p > 0.05$), indicating that high complexity does not mean greater performance.

5.3. Complexity

The number of trainable parameters for each model can be seen in Table 5. We note that, except for CNN-R, there has been a significant decrease in the number of algorithm parameters since the use of CNNs for P300 detection was first suggested. Especially since the introduction of EEGNet. The difference in parameters between OCLNN and FCNN is evident. The reduction is achieved because in the FCNN both neurons are connected to all the inputs of the network. In contrast, the convolutional block of the OCLNN selects a subset of feature maps to connect to the dense layer. On the other hand, the complexity reduction of SepConv1D is notorious and it is attributable to its depthwise convolution block.

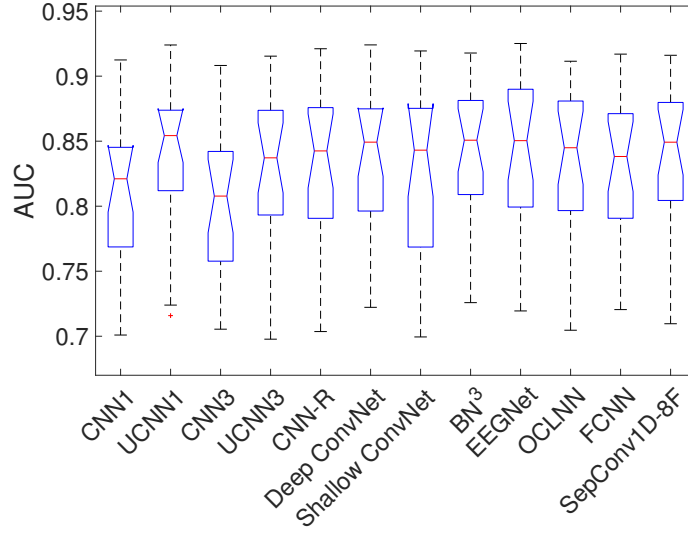


Figure 10: Mean AUC comparison between the models under analysis for cross-subject P300 detection. See detail in Table A.15.

Cecotti and Graser, 2011 [17]	CNN-1/UCNN-1	1,036,922
	CNN-3/UCNN-3	1,031,009
Manor y Geva, 2015 [18]	CNN-R	19,848,098
Schirrmeister et al., 2017 [20]	Deep ConvNet	178,077
	Shallow ConvNet	104,082
Liu et al., 2018 [21]	BN^3	44,633
Lawhern et al., 2018 [19]	EEGNet	2,338
Shan et al., 2018 [22]	OCLNN	1,842
Proposed	FCNN	2,477
	SepConv1D-1F	129
	SepConv1D-8F	353

Table 5: Number of trainable parameters per model.

6. Conclusions

In this paper, we presented SepConv1D, a simple Convolutional Neural Network architecture consisting of a depthwise separable 1D convolutional block followed by a Sigmoid classification block. The proposed architecture can solve a couple of problems that remain open in the BCI community: it can perform within-subject and cross-subject classification for P300 single-trial with the lowest computational cost compared to the state-of-the-art CNN-based methods.

Additionally, we provided elements to demonstrate that making the neural network deeper and highly complex does not lead to more accurate results when trying to solve the above-mentioned problems. To that end, we compared the performances of the state-of-the-art CNN-based methods against both one-hidden layer Fully-Connected Neural Network with two neurons and the SepConv1D.

The experiments were carried out on a 22-subject database. The results showed that the AUC values of both the FCNN and the SepConv1D were not statistically significantly different compared to the AUC values of the methods under analysis. The FCNN obtained an AUC of 0.8913 ± 0.05 for within-subject classification and 0.8283 ± 0.57 for cross-subject classification, whereas the SepConv1D obtained an AUC of 0.8903 ± 0.05 for within-subject classification and 0.8361 ± 0.59 for cross-subject classification. Moreover, SepConv1D has the lowest number of parameters of all by far: it uses 129 parameters for within-subject classification and 353 for cross-subject classification. The architecture with the closest number of parameters is the OCLNN with 1,842. This is important because it can be built simpler, cheaper, faster and, thus, more portable devices.

Appendix A.

References

- [1] J. Wolpaw, N. Birbaumer, W. J. Heetderks, D. J. McFarland, P. H. Peckham, G. Schalk, E. Donchin, L. A. Quatrano, C. J. Robinson, T. M. Vaughan, Brain-computer interface technology: A review of the first international meeting, IEEE Transactions on Rehabilitation Engineering 8 (2) (2000) 164–173.

Layer	No. filters	Size	No. params	Output	Activation function	Options
Input		206×6				
Conv1D	10	1	70	(206, 10)		padding = same, data format = "Channels last", bias and kernel initializer = **
Activation				(206, 10)	<i>stanh</i>	
Conv1D	50	13	6,550	(206, 50)		padding = same, data format = "Channels first", bias and kernel initializer = **
Activation				(206, 50)	<i>stanh</i>	
Flatten				(10, 300)		
Dense	100		1,030, 100	(100)	Sigmoid	
Dense	2		202	(2)	Sigmoid ¹ / Softmax ²	

Table A.6: CNN-1 and UCNN-1 architectures. ¹ CNN-1 uses Sigmoid activation. ² UCNN-1 uses Softmax activation.

Layer	No. filters	Size	No. params	Output	Activation function	Options
Input		206×6				
Conv1D	1	1	7	(206, 1)		padding = same, data format = "Channels last", bias and kernel initializer = **
Activation				(206, 1)	<i>stanh</i>	
Conv1D	50	13	700	(206, 50)		padding = same, data format = "Channels last", bias and kernel initializer = **
Activation				(206, 50)	<i>stanh</i>	
Flatten				(10, 300)		
Dense	100		1,030, 100	(100)	Sigmoid	
Dense	2		202	(2)	Sigmoid ¹ / Softmax ²	

Table A.7: CNN-3 and UCNN-3 architectures. ¹ CNN-3 uses Sigmoid activation. ² UCNN-3 uses Softmax activation.

Layer	No. filters	Size	No. params	Output	Activation function	Options
Input		206×6				
Conv1D	96	1	672	(206, 96)		activity regularizer ¹
Activation				(206, 96)	ReLU	
Max Pooling 1D	3	stride 2		(102, 96)		
Conv1D	128	6	73,856	(97, 128)		ReLU
Activation				(97, 128)	ReLU	
Max Pooling 1D	3	stride 2		(48, 128)		
Conv1D	128	6	98,432	(43, 128)		ReLU
Activation				(43, 128)	ReLU	
Flatten				(5, 504)		
Dense	2,048		11,274, 240	(2, 048)	ReLU	$p = 0.8$
Dropout				(2, 048)		
Dense	4,096		8,392,704	(4, 096)	ReLU	
Dropout				(4, 096)		$p = 0.8$
Dense	2		8,194	(2)		
Activation				(2)	Softmax	

Table A.8: CNN-R architecture. ¹ Activity regularizer = $0.01 \sum_{t=1}^{N-1} (a_{t+1}^{(l)} - a_t^{(l)})^2$, where $a_t^{(l)}$ is the convolution output at a time t in layer l .

Layer	No. filters	Size	No. params	Output	Activation function	Options
Input		6×206				
Reshape		$1 \times 6 \times 206$				
Conv2D	25	1×5	150	(25, 6, 202)		max norm = 2
Conv2D	25	6×1	40,025	(25, 1, 202)		max norm = 2
BatchNorm			100	(25, 1, 202)		
Activation				(25, 1, 202)	ELU	data format = "Channels first", $\epsilon = 1 \times 10^{-05}$, momentum = 0.1
MaxPool2D		1×2 pool size and stride		(25, 1, 101)		
Dropout				(25, 1, 101)		$p = 0.5$
Conv2D	50	1×5	6,300	(50, 1, 97)		max norm = 2
BatchNorm			200	(50, 1, 97)		
Activation				(50, 1, 97)	ELU	data format = "Channels first", $\epsilon = 1 \times 10^{-05}$, momentum = 0.1
MaxPool2D		1×2 pool size and stride		(50, 1, 48)		
Dropout				(50, 1, 48)		$p = 0.5$
Conv2D	100	1×5	25,100	(100, 1, 44)		max norm = 2
BatchNorm			400	(100, 1, 44)		data format = "Channels first", $\epsilon = 1 \times 10^{-05}$, momentum = 0.1
Activation				(100, 1, 44)	ELU	
MaxPool2D		1×2 pool size and stride		(100, 1, 22)		
Dropout				(100, 1, 22)		$p = 0.5$
Conv2D	200	1×5	100,200	(200, 1, 18)		max norm = 2
BatchNorm			800	(200, 1, 18)		data format = "Channels first", $\epsilon = 1 \times 10^{-05}$, momentum = 0.1
Activation				(200, 1, 18)	ELU	
MaxPool2D		1×2 pool size and stride		(200, 1, 9)		
Dropout				(200, 1, 9)		$p = 0.5$
Flatten				(1, 800)		
Dense	2		4,802	(2)	Softmax	max norm = 0.5

Table A.9: Deep ConvNet architecture. Version modified by [19].

Layer	No. filters	Size	No. params	Output	Activation function	Options
Input		6×206				
Reshape		$1 \times 6 \times 206$				
Conv2D	40	1×13	560	(40, 6, 194)		max norm constraint function = 2
Conv2D	40	6×1	9,600	(40, 1, 194)		max norm constraint function = 2, doesn't use bias
BatchNorm			160	(40, 1, 194)		axis to be normalized = 1, $\epsilon = 1 \times 10^{-05}$, momentum = 0.1
Activation				(40, 1, 194)	Square	
AveragePool2D		pool 1×35 , stride 1×7		(40, 1, 23)		
Activation				(40, 1, 23)	Log	$p = 0.5$
Dropout				(40, 1, 23)		
Flatten				(900)		
Dense	2		1,842	(2)	Softmax	max norm constraint function = 0.5

Table A.10: Shallow ConvNet architecture. Version modified by [19].

Layer	No. filters	Size	No. params	Output	Activation function	Options
Input				206×6		
BatchNorm			24	206×6		
Conv1D	16	1	112	206×16	ReLU	
Conv1D	16	20	5,136	11×16	ReLU	bias initializer = Glorot Uniform bias initializer = Glorot Uniform, strides = 20, padding = same
BatchNorm			64	11×16		
Activation				11×16	ReLU	
Flatten				176		
Dense		128	22,656	128	\tanh	bias initializer = Glorot Uniform $p = 0.8$
Dropout				128		
Dense		128	16,512	128	\tanh	bias initializer = Glorot Uniform $p = 0.8$
Dropout				128		
Dense	1		129	1	Sigmoid	bias initializer = Glorot Uniform

Table A.11: BN^3 architecture.

Layer	No. filters	Size	No. params	Output	Activation function	Options
Input				6×206		
Reshape				$1 \times 6 \times 206$		
Conv2D	8	1×64	512	(4, 6, 206)	Linear	padding = same, doesn't use bias
BatchNorm			16	(4, 6, 206)		
DepthwiseConv2D		6×1	48	(8, 1, 206)	Linear	doesn't use bias, number of depth-wise convolution output channels = 2, max norm constraint function = 1
BatchNorm			32	(8, 1, 206)		
Activation				(8, 1, 206)	ELU	
AveragePool2D		1×4		(8, 1, 51)		p
Dropout				(8, 1, 51)		
SeparableConv2D	16	1×16	192	(8, 1, 51)	Linear	padding = same, doesn't use bias
BatchNorm			32	(8, 1, 51)		
Activation				(8, 1, 51)	ELU	
AveragePool2D		1×8		(8, 1, 6)		p
Dropout				(8, 1, 6)		
Flatten				(48)		
Dense	2		98	(2)	Softmax	max norm constraint regularization = 0.25

Table A.12: EEGNet architecture, where $p = 0.25$ or 0.5 (for cross-subject or within-subject classification, respectively). Adapted from [19].

Layer	No. filters	Size	No. params	Output	Activation function	Options
Input		206×6				
ZeroPadding1D						
Conv1D	16	kernel and stride = 14	1,360	(210, 6) (15, 16)		padding = 2 kernel and bias regularizer use L2 = 0.01
Activation				(15, 16)	ReLU	
Dropout				(15, 16)		$p = 0.25$
Flatten				(240)		
Dense	2		482	(2)		
Activation				(2)	Softmax	

Table A.13: OCLNN architecture.

Table A.14: Mean AUCs of the models under analysis for within-subject P300 detection.

Subject	CNN1	UCNN1	CNN3	UCNN3	CNN-R	Deep Con-vNet	Shallow Con-vNet	BN^3	EEGNet	OCLNN	FCNN	SepConv1D-1F
ACS	0.9123	0.9165	0.6894	0.7288	0.8881	0.9118	0.8249	0.8981	0.8974	0.9113	0.919	0.9129
APM	0.9314	0.9347	0.7721	0.7919	0.9177	0.9398	0.899	0.926	0.9309	0.936	0.9327	0.93
ASG	0.908	0.9108	0.771	0.7795	0.9118	0.9218	0.8969	0.9087	0.9222	0.9139	0.9073	0.9149
ASR	0.7311	0.729	0.6263	0.6397	0.7147	0.7423	0.6675	0.7316	0.7421	0.7367	0.7311	0.7302
CLL	0.8479	0.8572	0.6453	0.6616	0.8126	0.8448	0.7267	0.834	0.8309	0.8441	0.8583	0.8478
DCM	0.9421	0.9458	0.8187	0.8621	0.9353	0.9503	0.9096	0.9442	0.9404	0.9467	0.943	0.9434
DLP	0.8042	0.8206	0.6171	0.6655	0.7903	0.83	0.7324	0.791	0.8224	0.8153	0.814	0.815
DMA	0.8516	0.8667	0.6755	0.709	0.8397	0.8655	0.7499	0.8474	0.8373	0.857	0.8641	0.8599
ELC	0.9077	0.9086	0.7526	0.813	0.8939	0.9164	0.8548	0.9008	0.9022	0.9064	0.9091	0.9105
FSZ	0.9035	0.9057	0.7347	0.7724	0.8896	0.9116	0.8602	0.8977	0.9065	0.9046	0.9062	0.9081
GCE	0.8674	0.8745	0.6963	0.7533	0.852	0.8742	0.8223	0.8659	0.8673	0.8757	0.8697	0.8696
ICE	0.8882	0.893	0.7108	0.7503	0.8776	0.9013	0.7757	0.8852	0.8763	0.8916	0.8931	0.8903
JCR	0.8577	0.8713	0.7078	0.7582	0.8505	0.8746	0.8038	0.8537	0.8623	0.8667	0.8672	0.8666
JLD	0.8931	0.8931	0.7383	0.8142	0.8877	0.9051	0.8582	0.891	0.8968	0.896	0.8938	0.8929
JLP	0.8773	0.8871	0.6724	0.7177	0.8745	0.899	0.8532	0.8817	0.8864	0.8821	0.8842	0.8878
JMR	0.9187	0.9244	0.7602	0.8377	0.9061	0.925	0.8797	0.9117	0.9151	0.9185	0.929	0.9211
JSC	0.8223	0.837	0.622	0.67	0.8081	0.8483	0.748	0.8233	0.8317	0.8379	0.8388	0.8361
JST	0.9675	0.9684	0.8433	0.9121	0.9635	0.9715	0.951	0.9641	0.9699	0.9681	0.9675	0.9677
LAC	0.9379	0.9485	0.8037	0.8599	0.9457	0.9524	0.9322	0.9413	0.9438	0.9497	0.9468	0.9427
LAG	0.933	0.9353	0.6993	0.8393	0.9289	0.9435	0.9158	0.9382	0.9412	0.9406	0.9323	0.9404
LGP	0.9288	0.9338	0.8228	0.8587	0.9268	0.9399	0.8939	0.9287	0.9339	0.934	0.9348	0.9354
LPS	0.863	0.8668	0.6406	0.764	0.8473	0.871	0.802	0.8617	0.8675	0.867	0.8666	0.8636

Table A.15: Mean AUCs of the models under analysis for cross-subject P300 detection.

Subject	CNN1	UCNN1	CNN3	UCNN3	CNN-R	Deep Con-vNet	Shallow Con-vNet	BN^3	EEGNet	OCLNN	FCNN	SepConv1D-1F
ACS	0.8527	0.8653	0.8392	0.8366	0.8545	0.8695	0.8151	0.8725	0.8685	0.8539	0.8554	0.8727
APM	0.8453	0.8615	0.3495	0.8442	0.8468	0.8569	0.8508	0.8652	0.8706	0.8552	0.8515	0.8627
ASG	0.8680	0.8914	0.8680	0.8878	0.8892	0.8995	0.8753	0.8813	0.8972	0.8741	0.8712	0.8917
ASR	0.7260	0.7240	0.7167	0.7146	0.7293	0.7237	0.7253	0.7268	0.7332	0.7244	0.7205	0.7247
CLL	0.7009	0.7159	0.7054	0.6977	0.7036	0.7222	0.7071	0.7258	0.7195	0.7046	0.7235	0.7096
DCM	0.8332	0.8960	0.8421	0.8903	0.8819	0.8901	0.8840	0.8860	0.8899	0.8900	0.8851	0.8806
DLP	0.7687	0.7998	0.7726	0.7742	0.7907	0.7856	0.7615	0.7984	0.7969	0.7709	0.7888	0.7939
DMA	0.7542	0.8119	0.7923	0.7962	0.7791	0.7963	0.7686	0.8090	0.7994	0.7741	0.7863	0.7998
ELC	0.8433	0.8738	0.8477	0.8613	0.8758	0.8600	0.8608	0.8818	0.8747	0.8809	0.8774	0.8798
FSZ	0.8204	0.8563	0.8315	0.8496	0.8392	0.8506	0.8480	0.8625	0.8590	0.8448	0.8488	0.8579
GCE	0.8018	0.8312	0.7782	0.7932	0.8206	0.8389	0.8435	0.8317	0.8379	0.8213	0.8074	0.8193
ICE	0.7664	0.7880	0.7577	0.7660	0.7816	0.7808	0.7538	0.7810	0.7907	0.7966	0.7956	0.8044
JCR	0.8350	0.8308	0.4988	0.8241	0.8458	0.8174	0.8117	0.8390	0.8213	0.8296	0.8266	0.8274
JLD	0.8650	0.8666	0.8326	0.8415	0.8664	0.8749	0.8568	0.8656	0.8715	0.8599	0.8491	0.8632
JLP	0.8079	0.8181	0.8014	0.8061	0.8333	0.8024	0.8081	0.8197	0.8065	0.8191	0.7907	0.8070
JMR	0.8007	0.8523	0.8374	0.8378	0.8192	0.8479	0.8427	0.8337	0.8419	0.8451	0.8277	0.8406
JSC	0.7306	0.7360	0.7221	0.7119	0.7511	0.7437	0.6995	0.7291	0.7286	0.7265	0.7338	0.7326
JST	0.9125	0.9194	0.9082	0.9154	0.9105	0.9148	0.9127	0.9052	0.9251	0.9115	0.9101	0.9111
LAC	0.8395	0.9240	0.7672	0.8940	0.9211	0.9240	0.9194	0.9178	0.9245	0.9025	0.9169	0.9161
LAG	0.8217	0.8722	0.8571	0.8737	0.8666	0.8623	0.9093	0.8737	0.8960	0.8841	0.8606	0.8775
LGP	0.8704	0.8951	0.8752	0.8937	0.8930	0.9022	0.8765	0.8994	0.8966	0.8952	0.8913	0.9006
LPS	0.7923	0.8339	0.8141	0.8157	0.8030	0.8080	0.8152	0.8199	0.8257	0.8325	0.8048	0.8204

- [2] E. Donchin, K. M. Spencer, R. Wijesinghe, The mental prosthesis: assessing the speed of a P300-based brain-computer interface, *IEEE transactions on rehabilitation engineering* 8 (2) (2000) 174–179.
- [3] N. E. L. da Silva F, *Electroencephalography: Basic Principles, Clinical Applications, and Related Fields*, 5th Edition, Lippincott Williams & Wilkins, 2005.
- [4] F. Lotte, L. Bougrain, A. Cichocki, M. Clerc, M. Congedo, A. Rakotomamonjy, F. Yger, A review of classification algorithms for EEG-based brain-computer interfaces: a 10 year update, *Journal of Neural Engineering* 15 (3) (2018) 031005.
- [5] D. J. Krusienski, E. W. Sellers, F. Cabestaing, S. Bayouth, D. J. McFarland, T. M. Vaughan, J. R. Wolpaw, A comparison of classification techniques for the P300 speller, *Journal of Neural Engineering* 3 (4) (2006) 299.
- [6] Y. Atum, I. Gareis, G. Gentiletti, R. Acevedo, L. Rufiner, Genetic feature selection to optimally detect P300 in brain computer interfaces, in: *Engineering in Medicine and Biology Society (EMBC), 2010 Annual International Conference of the IEEE, IEEE, 2010*, pp. 3289–3292.
- [7] V. Bostanov, BCI competition 2003-data sets Ib and IIb: feature extraction from event-related brain potentials with the continuous wavelet transform and the t-value scalogram, *IEEE Transactions on Biomedical engineering* 51 (6) (2004) 1057–1061.
- [8] M. Kaper, P. Meinicke, U. Grossekhoefer, T. Lingner, H. Ritter, BCI competition 2003-data set IIb: support vector machines for the P300 speller paradigm, *IEEE Transactions on Biomedical Engineering* 51 (6) (2004) 1073–1076.
- [9] L. Čechovič, M. Hodoň, M. Jurečka, P300 evoked potentials data classification using feed forward neural network, *European International Journal of Science and Technology* 2 (2) (2013) 5.
- [10] E. Abdulhay, R. Oweis, A. Mohammad, L. Ahmad, Investigation of a wavelet-based neural network learning algorithm applied to P300 based brain-computer interface, *Biomedical Research* (2017) S320–S324.

- [11] H. Woehrle, M. M. Krell, S. Straube, S. K. Kim, E. A. Kirchner, F. Kirchner, An adaptive spatial filter for user-independent single trial detection of Event-Related Potentials, *IEEE Transactions on Biomedical Engineering* 62 (7) (2015) 1696–1705.
- [12] T. Zeyl, E. Yin, M. Keightley, T. Chau, Partially supervised P300 speller adaptation for eventual stimulus timing optimization: target confidence is superior to error-related potential score as an uncertain label, *Journal of Neural Engineering* 13 (2) (2016) 026008.
- [13] L. Mayaud, S. Cabanilles, A. V. Langenhove, M. Congedo, A. Barachant, S. Pouplin, S. Filipe, L. Péténief, O. Rochecouste, E. Azabou, C. Hugeron, M. Lejaille, D. Orlikowski, D. Annane, Brain-computer interface for the communication of acute patients: a feasibility study and a randomized controlled trial comparing performance with healthy participants and a traditional assistive device, *Brain-Computer Interfaces* 3 (4) (2016) 197–215.
- [14] K. He, X. Zhang, S. Ren, J. Sun, Deep residual learning for image recognition, in: *2016 IEEE Conference on Computer Vision and Pattern Recognition (CVPR)*, 2016, pp. 770–778.
- [15] O. Abdel-Hamid, A. Mohamed, H. Jiang, L. Deng, G. Penn, D. Yu, Convolutional Neural Networks for Speech Recognition, *IEEE/ACM Transactions on Audio, Speech, and Language Processing* 22 (10) (2014) 1533–1545.
- [16] F. Lotte, Signal processing approaches to minimize or suppress calibration time in oscillatory activity-based Brain-Computer Interfaces, *Proceedings of the IEEE* 103 (6) (2015) 871–890.
- [17] H. Cecotti, A. Graser, Convolutional neural networks for P300 detection with application to brain-computer interfaces, *IEEE Transactions on Pattern Analysis and Machine Intelligence* 33 (3) (2011) 433–445.
- [18] R. Manor, A. B. Geva, Convolutional neural network for multi-category rapid serial visual presentation BCI, *Frontiers in Computational Neuroscience* 9 (146).

- [19] V. J. Lawhern, A. J. Solon, N. R. Waytowich, S. M. Gordon, C. P. Hung, B. J. Lance, EEGNet: A compact convolutional network for EEG-based brain-computer interfaces, *Journal of Neural Engineering* 15 (5) (2018) 056013.
- [20] R. T. Schirrmeister, J. T. Springenberg, L. D. J. Fiederer, M. Glasstetter, K. Eggersperger, M. Tangermann, F. Hutter, W. Burgard, T. Ball, Deep learning with convolutional neural networks for EEG decoding and visualization, *Human Brain Mapping* 38 (11) (2017) 5391–5420.
- [21] M. Liu, W. Wu, Z. Gu, Z. Yu, F. Qi, Y. Li, Deep learning based on Batch Normalization for P300 signal detection, *Neurocomputing* 275 (2018) 288–297.
- [22] H. Shan, Y. Liu, T. Stefanov, A simple convolutional neural network for accurate P300 detection and character spelling in brain computer interface, in: *Proceedings of the 27th International Joint Conference on Artificial Intelligence, IJCAI’18*, AAAI Press, 2018, pp. 1604–1610.
- [23] I. Goodfellow, Y. Bengio, A. Courville, *Deep Learning*, MIT Press, 2016.
- [24] S. Ioffe, C. Szegedy, Batch normalization: Accelerating deep network training by reducing internal covariate shift, in: *International Conference on Machine Learning*, 2015, pp. 448–456.
- [25] D. Scherer, A. Müller, S. Behnke, Evaluation of pooling operations in convolutional architectures for object recognition, in: K. Diamantaras, W. Duch, L. S. Iliadis (Eds.), *Artificial Neural Networks – ICANN 2010*, Springer Berlin Heidelberg, Berlin, Heidelberg, 2010, pp. 92–101.
- [26] I. H. Witten, E. Frank, M. A. Hall, C. J. Pal, Chapter 10 - deep learning, in: I. H. Witten, E. Frank, M. A. Hall, C. J. Pal (Eds.), *Data Mining (Fourth Edition)*, fourth edition Edition, Morgan Kaufmann, 2017, pp. 417 – 466.
- [27] Y. LeCun, Generalization and network design strategies, *Connectionism in perspective* (1989) 143–155.

- [28] V. Nair, G. E. Hinton, Rectified linear units improve restricted Boltzmann machines, in: Proceedings of the 27th International Conference on Machine Learning (ICML-10), 2010, pp. 807–814.
- [29] D. Clevert, T. Unterthiner, S. Hochreiter, [Fast and accurate deep network learning by exponential linear units \(elus\)](#), CoRR abs/1511.07289. [arXiv:1511.07289](#).
URL <http://arxiv.org/abs/1511.07289>
- [30] N. Srivastava, G. Hinton, A. Krizhevsky, I. Sutskever, R. Salakhutdinov, Dropout: A simple way to prevent neural networks from overfitting, *Journal of Machine Learning Research* 15 (2014) 1929–1958.
- [31] D. Kingma, J. Ba, Adam: A method for stochastic optimization, arXiv.
- [32] X. Glorot, Y. Bengio, Understanding the difficulty of training deep feedforward neural networks, in: Y. W. Teh, M. Titterton (Eds.), Proceedings of the Thirteenth International Conference on Artificial Intelligence and Statistics, Vol. 9 of Proceedings of Machine Learning Research, PMLR, Chia Laguna Resort, Sardinia, Italy, 2010, pp. 249–256.
- [33] C. Ledesma-Ramirez, E. Bojorges-Valdez, O. Yáñez-Suarez, C. Saavedra, L. Bougrain, G. G. Gentiletti, An open-access P300 speller database, Fourth International Brain-Computer Interface Meeting, poster (May 2010).
- [34] M. Alvarado-González, E. Garduño, E. Bribiesca, O. Yáñez-Suárez, V. Medina-Bañuelos, P300 detection based on EEG shape features, *Computational and mathematical methods in medicine* 2016 (2016) 14.
- [35] F. Chollet, et al., Keras, <https://github.com/fchollet/keras> (2015).
- [36] Martín, et al., [TensorFlow: Large-scale machine learning on heterogeneous systems](#) (2015).
URL <https://www.tensorflow.org/>